

Partially-Implicit Method for Fast Magnetization Analysis Using Assembled Domain Structure Model

Shogo Tejima¹, Shumpei Ito^{1,2}, Takeshi Mifune¹, *Member, IEEE*, Tetsuji Matsuo¹, *Member, IEEE* and Tomoo Nakai³

¹Kyoto University, Kyotodaigaku-katsura, Nishikyo-ku, Kyoto, 615-8510, Japan

²JSPS, Kojimachi Business Center Building, 5-3-1 Kojimachi, Chiyoda-ku, Tokyo 102-0083, Japan

³Industrial Technology Institute, Miyagi Prefectural Government, Sendai, 981-3206, Japan

A partially-implicit solution method is developed for fast magnetization analysis using an assembled domain structure model. The implicit time-marching scheme is simplified to avoid the inversion of a dense Jacobian matrix by separating the magnetostatic field into near and far components. The proposed approach achieves a reduction of computation time by 94 to 99%.

Index Terms—Implicit method, magnetic domain, multi-scale model, demagnetizing field.

I. INTRODUCTION

ADVANCED simulation technologies are being used in the computer-aided design of electric machines and electronic devices. Microscopic magnetic devices are also being designed using micro-magnetic simulations (MMSs) that solve the Landau-Lifshitz-Gilbert equation (LLGE) [1]–[4]. For macroscopic or mesoscopic magnetization analyses, however, the solution of LLGE requires huge computational cost because of the exchange-field computation on nanoscale cells. Recently, several energy-based multiscale approaches [5]–[7] have been studied to construct physical macroscale models and succeeded to reconstruct the magnetization property of silicon steel. Among them, the assembled-domain-structure model (ADSM) [7] can be applied to the mesoscopic analysis straightforwardly because it can handle the shape anisotropy due to the magnetostatic energy and the metastable magnetization states due to the magnetic anisotropy.

The ADSM consists of mesoscopic two (or six) domain cells. It was successfully applied to an analysis of thin-film giant magneto-impedance (GMI) elements [8] and silicon steels [7]. In the ADSM, a magnetization state that locally minimizes the total energy is determined using explicit time integration [9], although at large computational cost. This study develops a partially-implicit time-integration method to find local energy minima at small computational cost. The partial-implicit method is compared with the explicit method and also with another efficient ADSM based on magnetization-state switching in unit cells using the threshold fields [10] in an analysis of the GMI sensor.

II. PARTIALLY-IMPLICIT METHOD IN THE ADSM

A. Simplified domain structure model and its assembly

The simplified-domain-structure model (SDSM) is a mesoscopic magnetization model that represents the domain wall motion and magnetization rotation of two or six domains. Fig. 1(a) shows a schematic of the SDSM for two domains, where (ϕ_i, θ_i) is the spherical angles of the magnetization vector of domain i ($i = 1, 2$); λ_1 and $\lambda_2 = 1 - \lambda_1$ are their volume ratios.

The ADSM is a macroscopic magnetization model [Fig. 1(b)] constructed by assembling unit cells, each being a SDSM [8]. The magnetization is described by the collective behavior of the cells. The magnetization state of each cell is determined by the local minimization of the total magnetic energy consisting of the Zeeman energy, anisotropy energy, domain-wall energy, and magnetostatic energy [9].

The normalized total energy e of the ADSM is given as

$$e = e_{\text{ap-global}} + e_{\text{an-global}} + e_{\text{w-global}} + e_{\text{st-global}}, \quad (1)$$

where the Zeeman energy $e_{\text{ap-global}}$, the anisotropic energy $e_{\text{an-global}}$, and the domain-wall energy $e_{\text{w-global}}$ are the summations of the energy components of all cells. The magnetostatic energy $e_{\text{st-global}}$ is due to the magnetostatic field to be discussed in II.B.

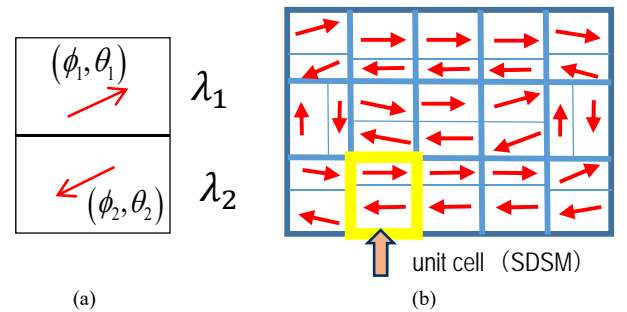


Fig. 1. Schematics of (a) the SDSM and (b) the ADSM.

The magnetization state of cell k is represented by the state variable vector $\mathbf{x}(k) = (\phi_1, \theta_1, \phi_2, \theta_2, \lambda_1)$. The magnetization vector \mathbf{X} in the ADSM consists of all the cell state variable vectors $\mathbf{x}(k)$ ($k = 1, 2, \dots$).

The local minimization of e is achieved by solving the ordinary differential equation (ODE) given by

$$\left(\frac{d\mathbf{X}}{dt}, \frac{d\mathbf{Y}}{dt} \right) = \mathbf{F}(\mathbf{X}, \mathbf{Y}) = (\mathbf{Y}, -\gamma\mathbf{Y} - \frac{\partial e}{\partial \mathbf{X}}) \quad (2)$$

where γ is the coefficient of dissipation and \mathbf{Y} is an intermediate variable vector. Equation (2) is an artificial state equation for \mathbf{X} and \mathbf{Y} . A local energy minimum is obtained by

numerically integrating (2) until reaching an equilibrium point where $\frac{dX}{dt} = \frac{dY}{dt} = 0$ (see Appendix for detail). The obtained equilibrium point depends on the initial conditions, meaning it depends on the magnetization history.

B. Partially-implicit method

The forward Euler method is often used to solve ODEs, but it is necessary to reduce significantly the step size if the ODE is stiff. In that case, an implicit scheme such as the backward Euler method is effective.

The implicit time-integration of (2) requires the Hessian matrix $\partial^2 e / \partial X^2$. As the magnetostatic field depends on all the cells' dipoles, the Hessian matrix becomes dense. This incurs a large computational cost if the number of cells is large because the nonlinear solution by the Newton–Raphson iteration requires the inversion of the Jacobian matrix including the Hessian matrix.

A partially- or semi-implicit scheme [3], [4] is sometimes used in the MMSs to solve the LLGE efficiently. In most cases, the magnetostatic field is not handled implicitly but processed explicitly to avoid the full matrix inversion. In this study, however, the magnetostatic field is one of the dominant terms to be handled implicitly. This paper proposes the decomposition of magnetostatic field as below.

The demagnetizing field $\mathbf{h}_{st}(i)$ is obtained by convolution

$$\mathbf{h}_{st}(i) = \sum_{i'} \mathbf{s}(i - i') \mathbf{m}(i'), \quad (3)$$

where i is the cell index, \mathbf{s} the demagnetizing coefficient matrix, and $\mathbf{m}(i')$ the magnetization vector of cell i' . Here $\mathbf{h}_{st}(i)$ is divided into near field $\mathbf{h}_{stin}(i)$ and far field $\mathbf{h}_{stex}(i)$, where $\mathbf{h}_{stin}(i)$ and $\mathbf{h}_{stex}(i)$ are generated by cell i and by the other cells, respectively [10], [11]. They are given by

$$\begin{aligned} \mathbf{h}_{stin}(i) &= \mathbf{s}(0) \mathbf{m}(i), \\ \mathbf{h}_{stex}(i) &= \sum_{i' \neq i} \mathbf{s}(i - i') \mathbf{m}(i') = \sum_{i'} \mathbf{s}'(i - i') \mathbf{m}(i'), \end{aligned} \quad (4)$$

$$\mathbf{s}'(i) = \begin{cases} 0 & (i = 0) \\ \mathbf{s}(i) & (i \neq 0) \end{cases}.$$

In the partially-implicit scheme, $\mathbf{h}_{stex}(i)$ is temporally integrated by an explicit scheme whereas $\mathbf{h}_{stin}(i)$ is processed by an implicit scheme based on the fact that $\mathbf{s}'(i)$ is smaller than $\mathbf{s}(0)$. The time integration scheme is written as

$$(\mathbf{X}^{n+1}, \mathbf{Y}^{n+1}) = (\mathbf{X}^n, \mathbf{Y}^n) + \Delta t \mathbf{F}_{im}(\mathbf{X}^{n+1}, \mathbf{Y}^{n+1}) + \Delta t \mathbf{F}_{ex}(\mathbf{X}^n) \quad (5)$$

where Δt is the time-step and n is the time-index; \mathbf{F} is decomposed as $\mathbf{F}(\mathbf{X}, \mathbf{Y}) = \mathbf{F}_{im}(\mathbf{X}, \mathbf{Y}) + \mathbf{F}_{ex}(\mathbf{X})$; \mathbf{h}_{stex} is included in \mathbf{F}_{ex} and all the other terms of \mathbf{F} are included in \mathbf{F}_{im} . This method approximates the Hessian matrix in a block-diagonal form corresponding to each cell, and proceeds cell-by-cell with the implicit time-integration.

III. MAGNETIZATION ANALYSIS

This section presents results of the magnetization analysis using the ADSMs applying the Euler method (ADSM-E) and applying the partially-implicit method (ADSM-I).

A thin film GMI sensor with in-plane uniaxial-inclined easy axis is analyzed. It has three magnetization states (Fig. 2).

When the applied magnetic field is weak, stripe domains parallel to the easy axis direction are observed (labeled WM). When the magnetic field exceeds a threshold field, a single domain state (S+ or S−) appears due to the shape anisotropy. The magnetization state transition can be used as a memory in highly sensitive magnetic field detection [12], [13]. For this paper, an amorphous $\text{Co}_{85}\text{Nb}_{12}\text{Zr}_3$ film is examined with the easy axis direction $\theta_{\text{easy}} = 20^\circ$ due to the induced anisotropy. The film size is given in Fig. 2. The material parameter settings are: $\mu_0 M_s = 0.93$ T, exchange stiffness constant $A = 1.49 \times 10^{-11}$ J/m, and anisotropy constant $K_1 = 260$ J/m³.

Using the explicit scheme, [8] revealed the property of GMI element comparing the influence of perpendicular magnetic field with that of longitudinal distribution of magnetic field. In this paper, some of results are recomputed by the partially implicit scheme to compare the computation time and simulation accuracy with those given by the explicit method.

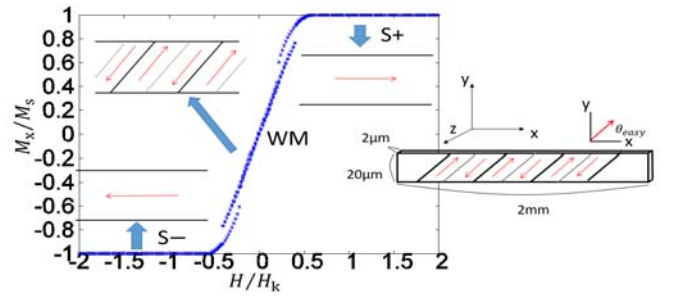


Fig. 2. Magnetization curves for the three states of a GMI film.

A. Magnetization analysis using the ADSM with 3 variables

First, assuming in-plane magnetization, the state variable vector $\mathbf{x}(k) = (\phi_1, \phi_2, \lambda_1)$ is used in each cell of the ADSM. The GMI film is divided into $64 \times 1 \times 1$ cells. Fig. 3 shows the magnetization M_x of the thin film with uniform applied magnetic field H along the longitudinal direction, where M_x and H are normalized by M_s and the anisotropy field $H_k = 2K_1 / \mu_0 M_s$, respectively. No significant difference is found in the simulated magnetizations obtained by the ADSM-E and ADSM-I (Fig. 3). Fig. 4 presents a comparison of the computation time taken for the ADSM-E and ADSM-I simulations; ADSM-I achieves a reduction of more than 99%.

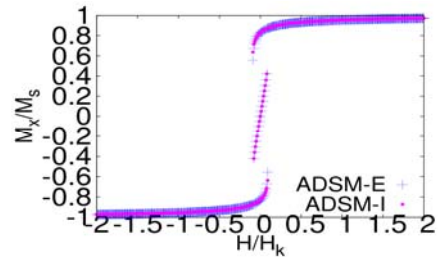


Fig. 3. Comparison of magnetization curves obtained using ADSM-I and ADSM-E.

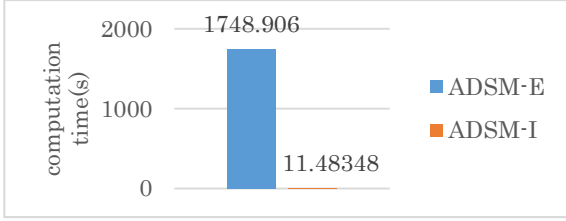


Fig. 4. Comparison of computation times of the ADSM-E and the ADSM-I simulations using 3 variables per cell.

B. Magnetization analysis using the ADSM with 5 variables

Next, to take into account an off-plane rotation, the state variable vector $\mathbf{x}(k) = (\phi_1, \theta_1, \phi_2, \theta_2, \lambda_1)$ is used in each cell of the ADSM. Fig. 5 compares the magnetization curves obtained by the ADSM-I and the ADSM-E, where the GMI film is divided into $64 \times 1 \times 1$ cells. Both methods yield almost the same magnetization as the 3-variable case. The threshold field for the transition from the negative single domain state (S⁻) to the positive single domain state (S⁺) is about 0.1 corresponding to the applied field of 56 A/m. The threshold field reported in [12] is about 40 A/m, which is sensitively affected by the film geometry and the easy axis direction and roughly agrees with the value from the simulation. Fig. 6(a) and (b) describe the magnetization property with the applied magnetic field distributed along the longitudinal direction as

$$H(x)/H_k = H_{ave}/H_k + h_1 x/L \quad (6)$$

where H_{ave} is the average magnetic field, $h_1 = 0.5, 1$ and $L = 1$ mm. For a distributed field with $h_1 = 1$, only the WM state is seen when $|H_{ave}|$ is small as is experimentally found in [13].

Fig. 7 compares computation times taken for the ADSM-E and the ADSM-I simulations of the GMI film in a uniform magnetic field. ADSM-I achieves a reduction of 94%.

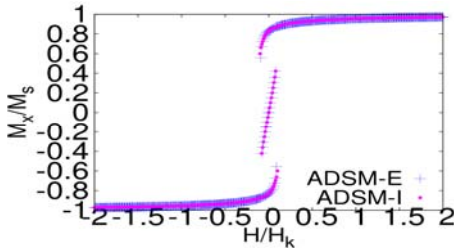


Fig. 5. Comparison of the magnetization curves obtained from the ADSM-I and ADSM-E simulations with 5 variables per cell.

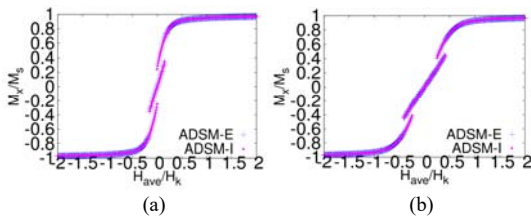


Fig. 6. Comparison of the magnetization curves obtained by the ADSM-E and the ADSM-I simulations for a magnetic field linearly distributed within (a) $h_1 = 0.5$ and (b) $h_1 = 1$.

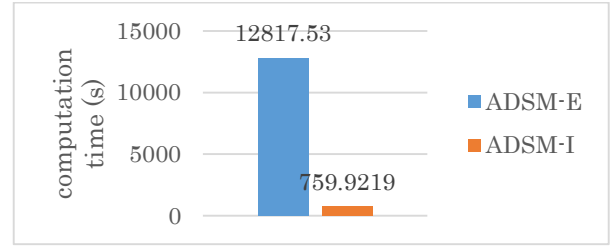


Fig. 7. Comparison of computation times for the ADSM-E and the ADSM-I simulations for a GMI film in a uniform magnetic field with 5 variables per cell.

C. Comparison with another efficient ADSM

This section aims a further reduction of computational cost by using another efficient method proposed in [10]. This method obtains the equilibrium point in each cell directly cell-by-cell. Similar to the ADSM-I, the magnetostatic field is divided into \mathbf{h}_{stin} and \mathbf{h}_{stex} , and \mathbf{h}_{stex} is added to the applied field \mathbf{h}_{ap} in cell k as $\mathbf{h}_{eff}(k) = \mathbf{h}_{ap} + \mathbf{h}_{stex}(k)$. The magnetization property given by the SDSM that constitutes the ADSM is assumed to be known. Then the magnetization state in cell k can be determined from $\mathbf{h}_{eff}(k)$. For the GMI film, the SDSM generates two types of magnetization states; a single domain state (S⁺ and S⁻ states) and the state of 180° domain-wall motion (WM state). If the threshold fields that induce the state transitions between S[±] and WM are known, the magnetization state in cell k can be switched depending on the variation of $\mathbf{h}_{eff}(k)$. The macroscopic magnetization is obtained by synthesizing the magnetizations of the unit cells (SDSMs), where the magnetization of cell k is determined by the effective field $\mathbf{h}_{eff}(k)$. This method is called ADSM-TS (threshold switching).

Fig. 8 compares the magnetization curves obtained by the ADSM-TS and the ADSM-I simulations. There is some difference between the simulated magnetization curves. This is because the ADSM-TS does not take into account the magnetization rotation exactly. When the applied magnetic field $|h| \leq 2$, the ADSM-I exhibits an ineligible magnetization rotation whereas the ADSM-TS does not give the magnetization rotation because a simple state transition between S[±] and WM is assumed.

A comparison of computation times (Fig. 9) show that the ADSM-TS achieves a reduction of 87% compared with ADSM-I but at the expense of some modeling accuracy.

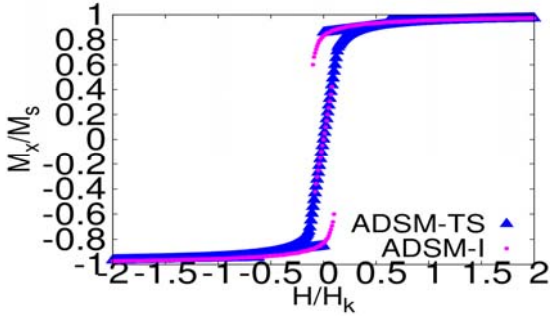


Fig. 8. Comparison of the magnetization curves for ADSM-TS and ADSM-I.

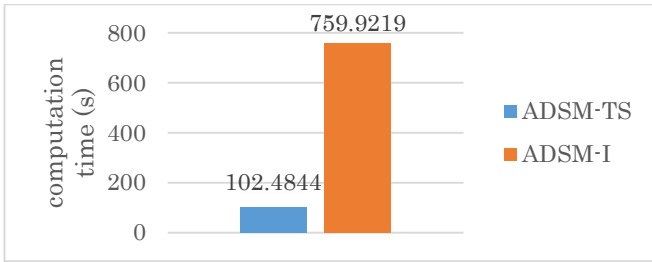


Fig. 9. Comparison of computation times for ADSM-TS and ADSM-I.

IV. CONCLUSION

A partially-implicit method for the ADSM was proposed, where the magnetostatic field is separately processed implicitly and explicitly to avoid a dense matrix inversion encountered in the Newton–Raphson iteration. The proposed method is more than 15 times as fast as the explicit method.

Another fast method called ADSM-TS reduces considerably the computation time but at the expense of modeling accuracy. This aspect needs to be addressed and improved if the method is to have use in practical simulations.

APPENDIX

A simple minimization of energy e is achieved by solving the ODE given as

$$\frac{d\mathbf{X}}{dt} = -\frac{\partial e}{\partial \mathbf{X}} \quad (7)$$

which corresponds to the steepest descent method. However, it sometimes fails because of an oscillation of \mathbf{X} in the solution process. The solution using (2) can be regarded as a gradient descent method with a momentum [14]. Equation (2) is an analogy of equation of motion driven by a potential energy e , which is described as $m d^2\mathbf{r}/dt^2 + \gamma d\mathbf{r}/dt + \partial e/\partial \mathbf{r} = 0$ where m is the mass and γ is the damping factor. In our case, however, the generalized mass and damping factor matrices for \mathbf{X} are not known. This is why we call (2) “artificial.” Equation (2) has equilibrium points where $\partial e/\partial \mathbf{X} = 0$. Their characteristic exponents are given by $[-\gamma \pm (\gamma^2 - 4\alpha)^{1/2}] / 2$ corresponding to an eigenvalue α of $\partial^2 e/\partial \mathbf{X}^2$. Hence, an equilibrium point is stable if all the eigenvalues of $\partial^2 e/\partial \mathbf{X}^2$ are positive; it is unstable if one of the eigenvalues is negative.

The partially implicit scheme is also effective to solve (7). The implicit solution of (7) is called ADSM-SD here. Fig. 10

compares its computation time with that by the ADSM-I, where the ADSM-I is faster than the ADSM-SD by 30 %.

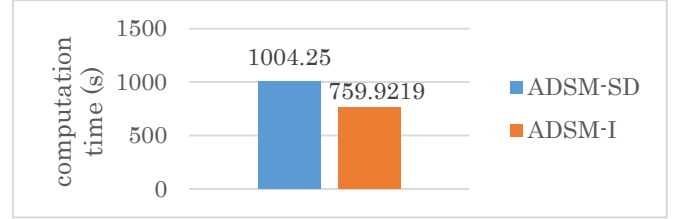


Fig. 10. Comparison of computation times for ADSM-SD and ADSM-I.

ACKNOWLEDGMENT

The authors express their gratitude to Prof. K. Ishiyama, Tohoku University, for his insightful comments on the magnetization analysis of thin-film GMI sensors. Part of this work was performed under the Cooperative Research Project Program of the Research Institute of Electrical Communication, Tohoku University.

REFERENCES

- [1] G. Bertotti, *Hysteresis in Magnetism*. San Diego, CA, USA: Academic Press, 1998.
- [2] H. Kronmüller and M. Fähnle, *Micromagnetism and Microstructure of Ferromagnetic Solids*. Cambridge University Press, 2003.
- [3] M. d’Aquino, C. Serpico, G. Mianol, I. D. Mayergoyz, and G. Bertotti, “Numerical integration of Landau-Lifshitz-Gilbert equation based on the midpoint rule,” *J. Appl. Phys.*, vol. 97, 10E319, 2005.
- [4] A. Furuya, J. Fujisaki, K. Shimizu, Y. Uehara, T. Ataka, T. Tanaka, and H. Oshima, “Semi-implicit steepest descent method for energy minimization and its application to micromagnetic simulation of permanent magnets,” *IEEE Trans. Magn.*, vol. 51, 2103004, 2015.
- [5] K. J. Rizzo, O. Hubert, and L. Daniel, “Magnetic and magnetostrictive behavior of iron-silicon single crystals under uniaxial stress,” *IEEE Trans. Magn.*, vol. 46, pp. 270-273, 2010.
- [6] A. Furuya, J. Fujisaki, Y. Uehara, K. Shimizu, H. Oshima, and T. Matsuo, “Micromagnetic hysteresis model dealing with magnetization flip motion for grain-oriented silicon steel,” *IEEE Trans. Magn.*, vol. 50, 7300604, 2014.
- [7] S. Ito, T. Mifune, T. Matsuo, and C. Kaido, “Macroscopic magnetization modeling of silicon steel sheets using an assembly of six-domain particles,” *J. Appl. Phys.*, vol. 117, 17D126, 2015.
- [8] S. Tejima, S. Ito, T. Mifune, T. Matsuo, and T. Nakai, “Magnetization analysis of stepped giant magneto impedance element using assembled domain structure model,” *Int. J. Appl. Electrom.*, vol. 52, pp. 541-546, 2016.
- [9] M. Sudo, T. Mifune, T. Matsuo, and C. Kaido, “A simplified domain structure model exhibiting the pinning field,” *IEEE Trans. Magn.*, vol. 49, pp. 1829-1832, 2013.
- [10] T. Matsuo, T. Nakamura, S. Ito, T. Mifune, and C. Kaido, “Efficient methods for macroscopic magnetization simulation described by the assembly of simplified domain structure models,” *Advanced Electromagnetics*, vol. 4, pp. 16-21, 2015.
- [11] T. Nakamura, S. Ito, T. Mifune, T. Matsuo, and C. Kaido, “Representation of magnetization process based on bifurcation property of domain structure,” *J. Appl. Phys.*, vol. 117, 17E516, 2015.
- [12] T. Nakai and K. Ishiyama, “Impedance variation with subjecting to normal field for the stepped giant magneto-impedance element,” *IEEE Trans. Magn.*, vol. 50, 4000904, 2014.
- [13] T. Nakai, “Magnetic domain observation of stepped giant magneto-impedance sensor with subjecting to normal magnetic field,” *Proc. IEEE Sensors 2015*, Busan, 2015.
- [14] N. Qian, “On the momentum term in gradient descent learning algorithms,” *Neural Networks*, vol. 12, pp. 145-151, 1999.